Electronic Supplementary Material (ESI) for Polymer Chemistry.

Supplementary Information

Broad-Spectrum Lignin-based Adhesives Using Thiol-Silyl Ether Crosslinkers

Yishayah Bension, Siteng Zhang, Tristan Menninger, Ting Ge*, Chuanbing Tang*

Department of Chemistry and Biochemistry, University of South Carolina, Columbia, South Carolina, 29208, United States.

*Corresponding Author Email: tang4@mailbox.sc.edu (C.T); tingg@mailbox.sc.edu (T.G.)

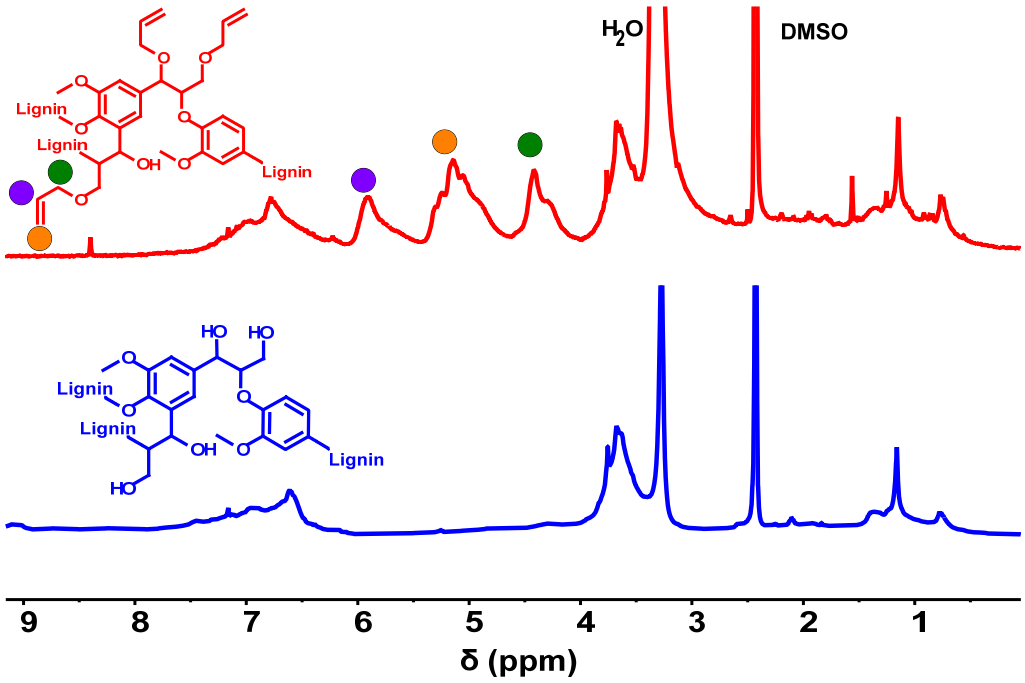

Figure S1. ^{1}H NMR spectra of allylated lignin (red) and organosolv lignin (blue).

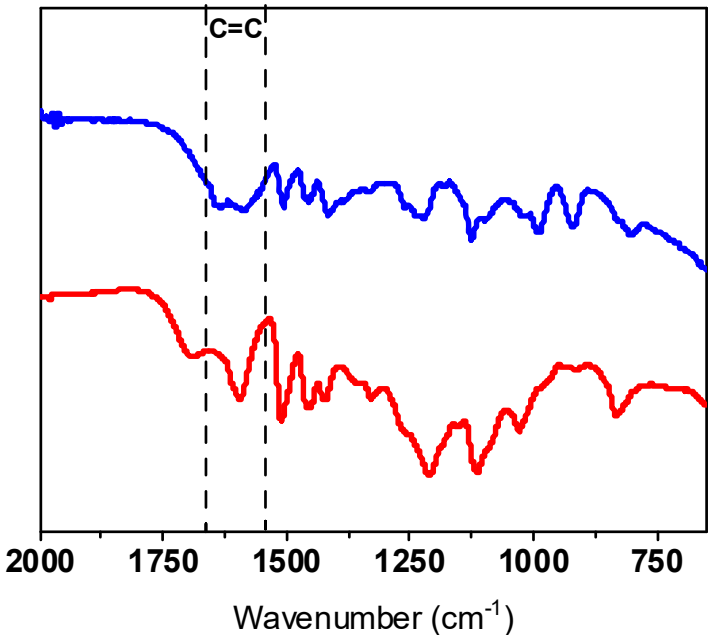

Figure S2. FTIR spectra of allylated lignin (red) and organosolv lignin (blue)

Lignin Hydroxyl Groups Quantification

2–chloro-4,4,5,5-tetramethyl-1,3,2-dioxaphospholane was used to quantify the hydroxyl groups and N-hydroxy-5-norbornene-2,3-dicarboximide was used as an internal standard following a previously published procedure.[1] The results from the lignin phosphorylation experiment are presented in figure S1 and table S1.

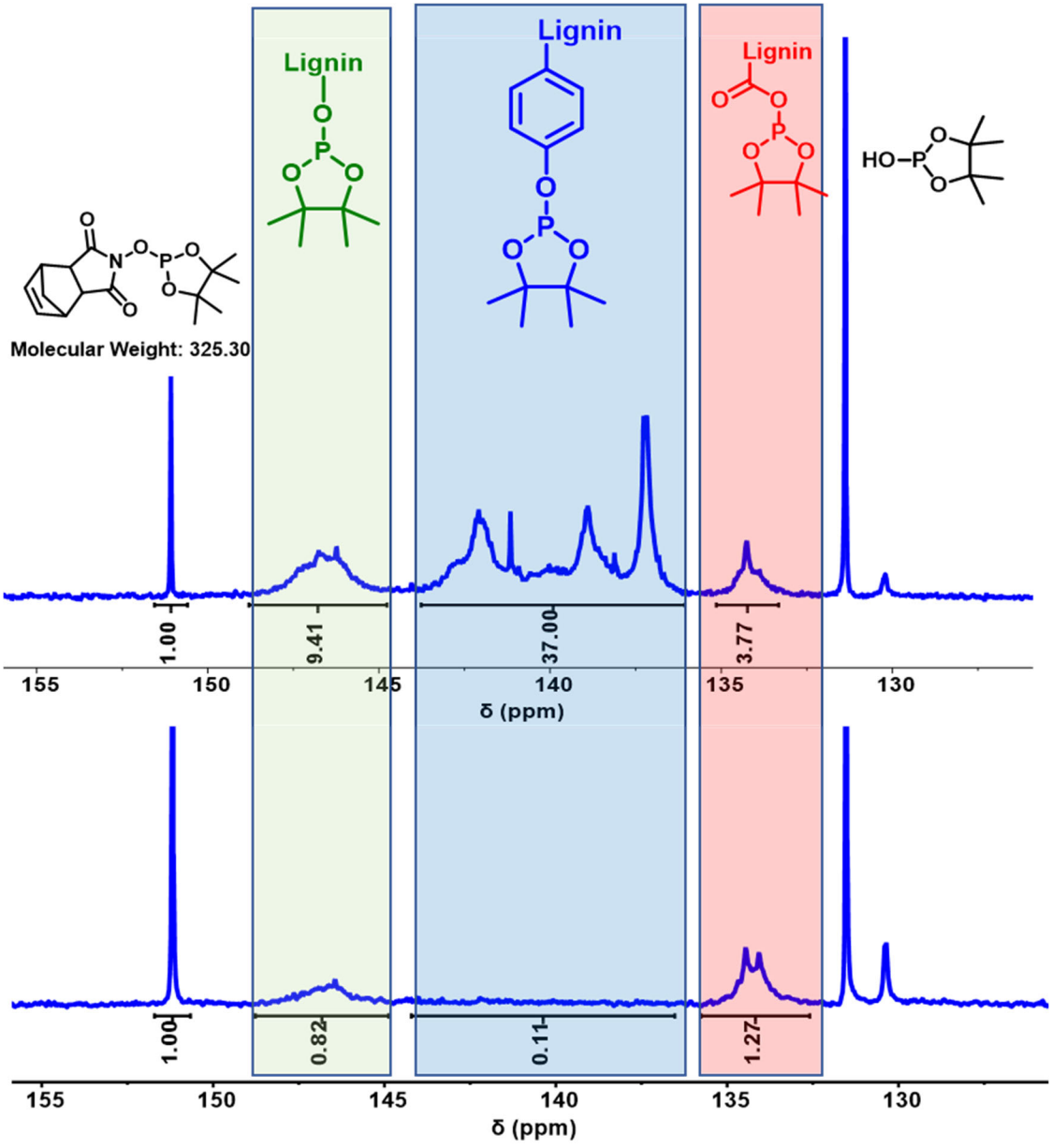

Figure S3. ^{31}P NMR spectral analysis of different hydroxyl and carboxylic acid groups: Top) Organosolv lignin; Bottom) Allylated lignin.

Table S1. ^{31}P NMR quantification of hydroxyl groups and carboxylic acid in lignin.

Lignin	Aliphatic alcohol (mmol/g)	Phenolic alcohol (mmol/g)	Carboxylic acid (mmol/g)
Organosolv	1.1	4.2	0.3
Allylated	0.1	~ 0.0	0.1

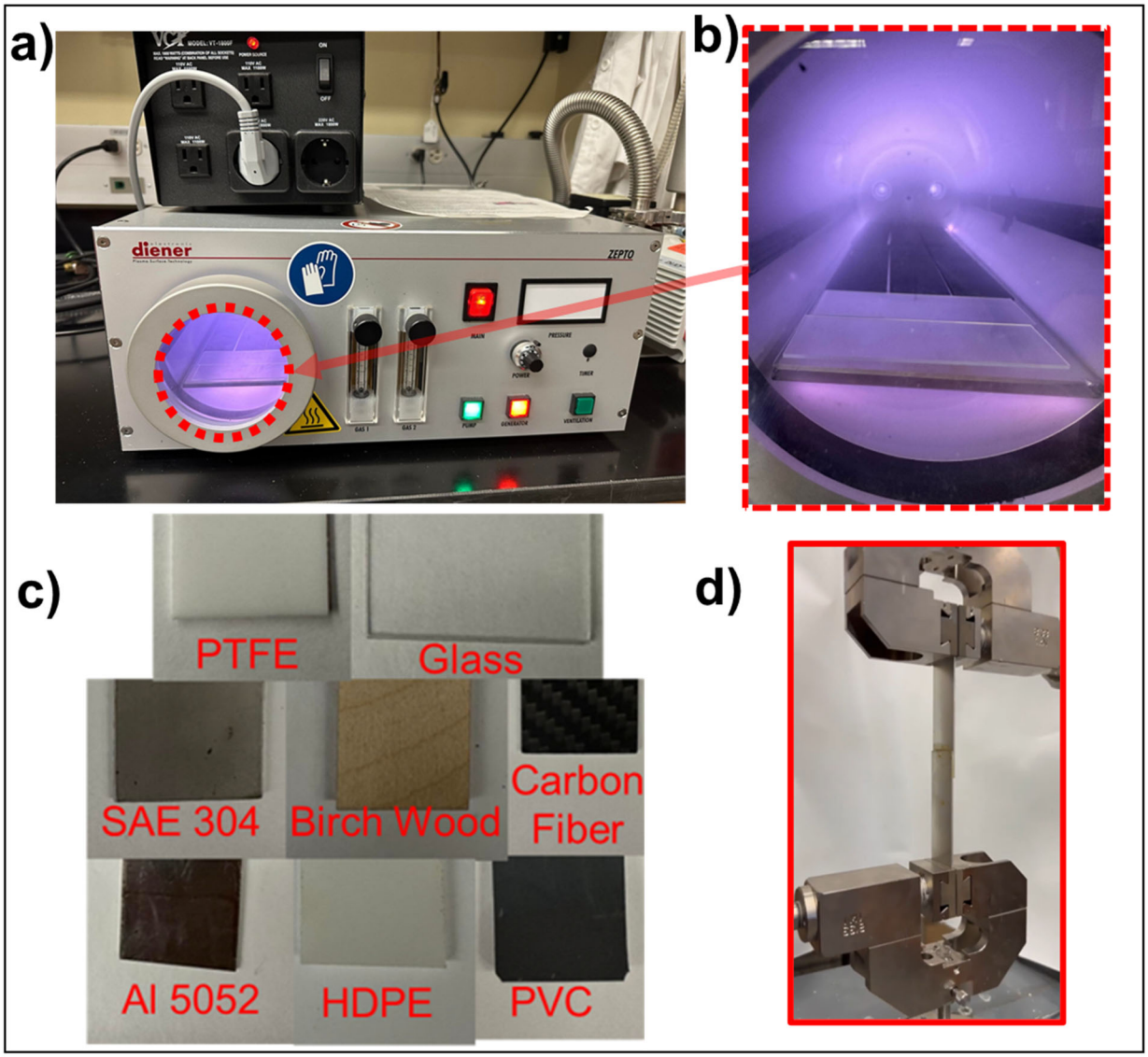

Figure S4. Optical images of experimental setup for; (a) plasma cleaning of substrates; (b) close up view of plasma chamber; (c) substrates tested; and (d) Lap-shear testing of adhesive on steel.

Molecular Dynamics Simulations

The simulation focused on the lignin-cellulose interface, which models the interface between lignin and wood. The miscanthus lignin sample from LigninBuilder was adapted to generate the lignin part in the simulation.[2] The cellulose substrate corresponds to the (100) surface of the I- β phase of crystalline cellulose, which has the highest areal density of hydroxyl groups compared to other crystalline surfaces. The cellulose substrate was created with the aid of CelluloseBuilder.[3] The classical CHARMM force field was used in the simulation.[4] The simulation sample was thoroughly equilibrated at constant temperature T=300 K and constant pressure P=1 atm for 1 ns. The simulation was performed using the LAMMPS package.[5]

The adhesion energy of lignin-cellulose interface was calculated as the difference of total energy (as shown in **Figure S5**) and the sum of two individual energies for the lignin matrix and cellulose substrate, respectively,

$$E_{adhesion} = E_{total} - (E_{substrate} + E_{lignin}) \quad \textbf{(1)}$$

The average E_adhesion over a molecular dynamics trajectory of 1 ns was computed and reported.

To understand the adhesion mechanism, we performed molecular dynamics simulations on the interface between lignin and cellulose. Cellulose was chosen because it is a major component of wood and the adhesion strength for the lignin-wood interface is among the strongest (**Figure 4**). Additionally, the cellulose surface has multiple polar groups that could potentially participate in nonbonding interactions with the lignin. The (100) surface of I-β cellulose crystal was simulated as it has a higher density of alcohol groups compared with other crystalline planes. The simulations were non-reactive, and therefore the curing mechanism, which requires a detailed modeling of bond formation and scission, was not explored. Instead, the simulations studied the nonbonding interactions including the van der Waals and electrostatic interactions to evaluate their roles in adhesion.

The interfacial energy between raw lignin and cellulose was calculated (**Figure S5**) to be (100 ± 9) mJ/m^2 using Equation (1) (see the experimental part). The result agrees with other simulation studies of lignin-cellulose interfaces.[6] This interfacial energy is weak compared to adhesion strength based on covalent bonding interactions. Using a conservative estimate of the covalent bond energy as 100 kJ/mol, the interfacial energy of 100 mJ/m^2 is converted to 1 covalent

bond per area of 13Å^2.[7] In contrast, a cured system may have at least 6 covalent bonds in the same interfacial area, assuming each bond of length 1.5 Å occupies an area of 2.25 Å^2. As a result, the adhesive's nonbonding interactions alone are not enough to explain the high adhesive strength observed experimentally in the cured system.

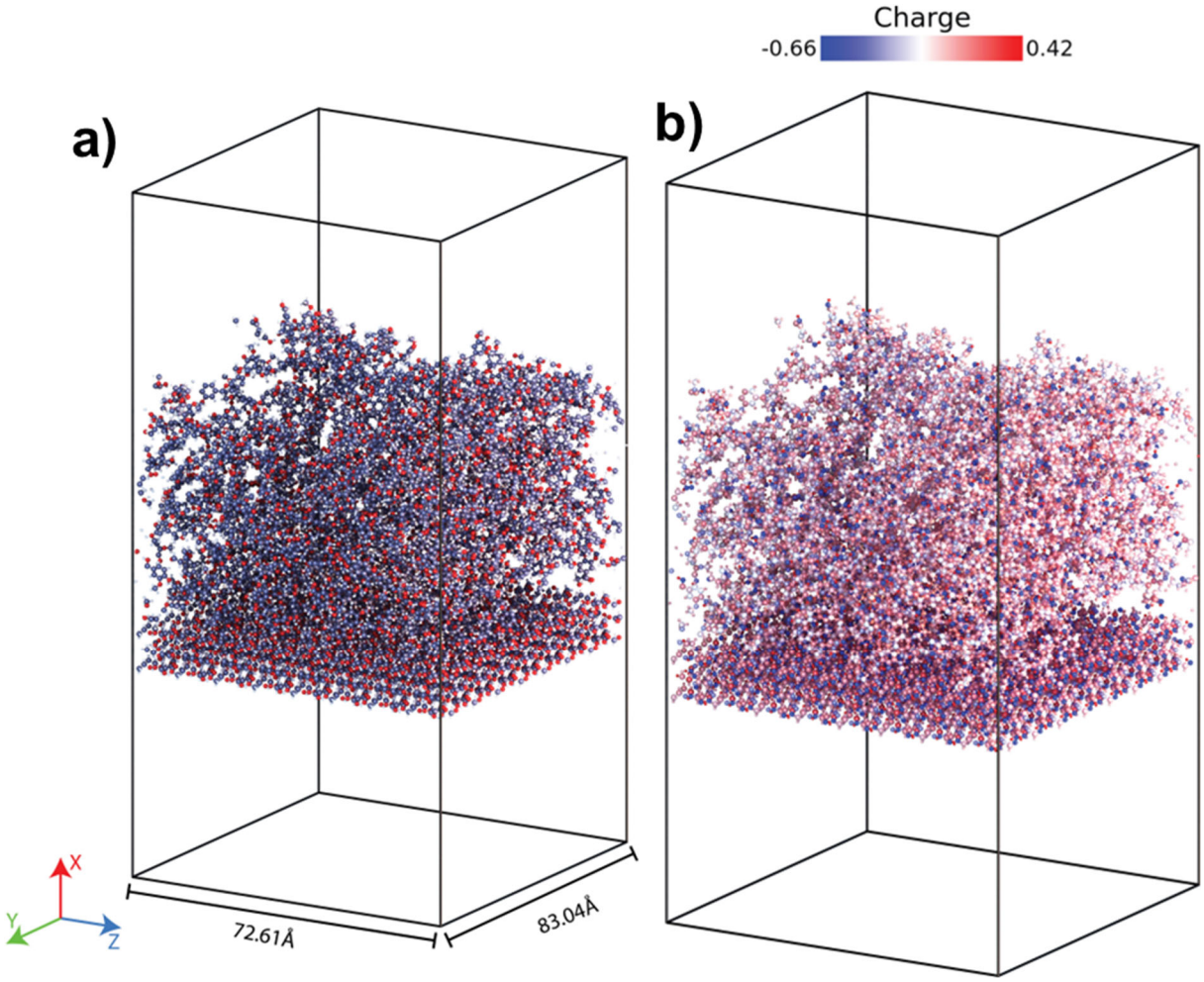

Figure S5. a) Snapshots of the interface between lignin and cellulose in the molecular dynamics simulation, where carbon, oxygen, and hydrogen are shown as grey, red, and white spheres, respectively; b) charge distribution in the simulated system.

NMR Spectra

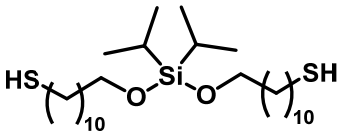

(11,11'-((diisopropylsilanediyl)bis(oxy))bis(undecane-1-thiol))

Yield: 94%. **^{1}H NMR** (400 MHz, $CDCl_3$) δ = 1-1.56 (m, 50H), 2.54 (q, -C**H_2**-SH, 4H), 3.66 (t, -O-C**H_2**-, 4H). **^{13}C NMR** (400 MHz, $CDCl_3$) δ 12.3, 17.5, 24.8, 25.9, 28.5, 29.2, 29.6, 29.7, 29.7, 29.8, 33.0. 34.2, 63.1. **^{29}Si NMR:** (400 MHz, $CDCl_3$) δ = -11.

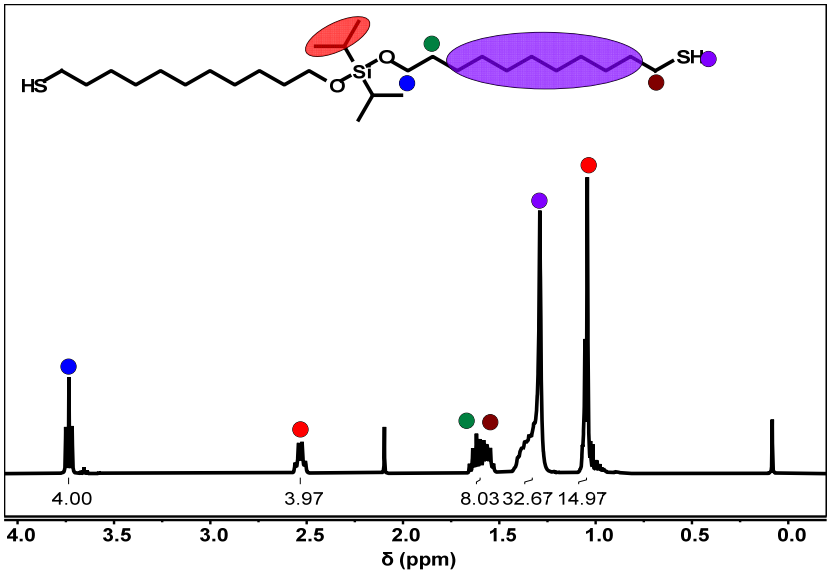

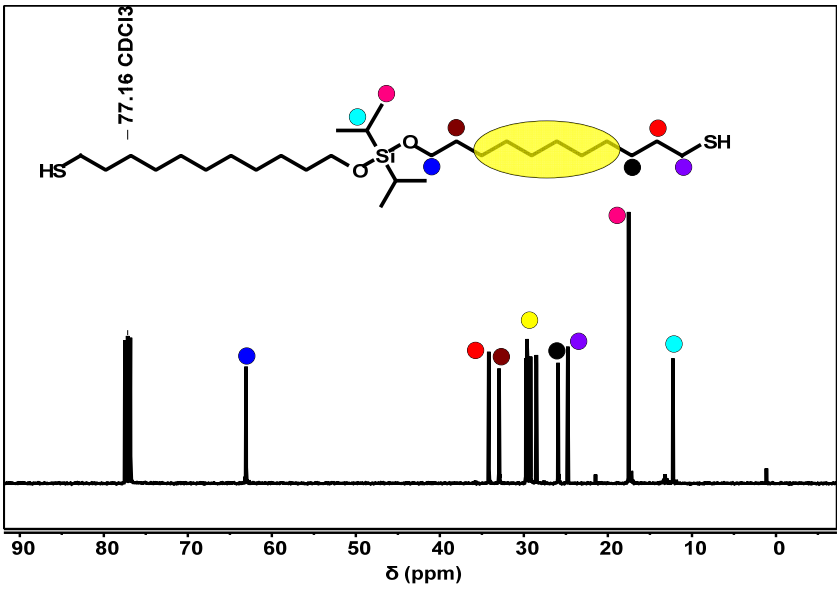

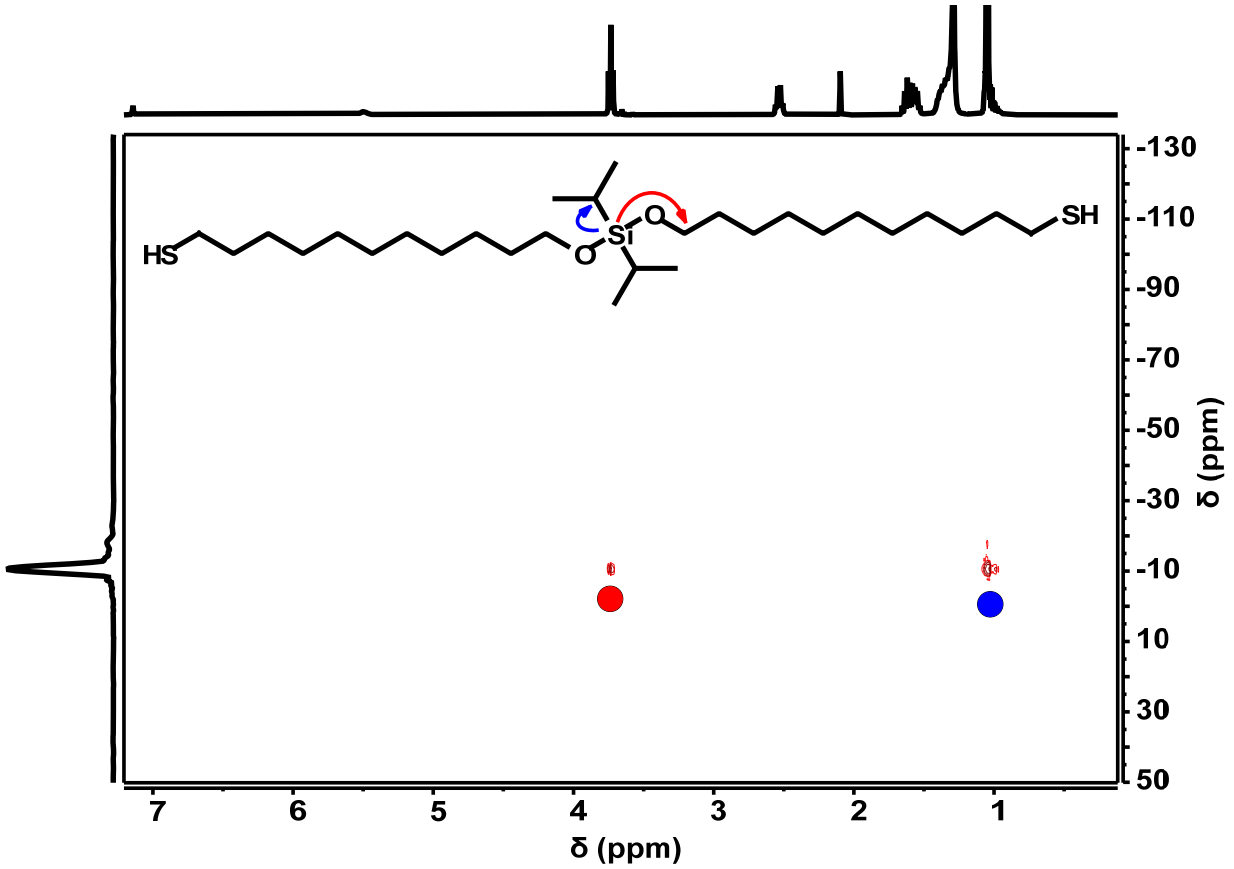

Figure S6. ^{1}H (Top), ^{13}C (Middle), and ^{1}H - ^{29}Si HMBC (Bottom) NMR spectra of (11,11'-((diisopropylsilanediyl)bis(oxy))bis(undecane-1-thiol)).

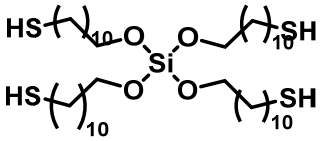

TSE-11 tetrakis(11-mercaptoundecyl) silicate

Yield: 90 %. **^{1}H NMR** (400 MHz, $CDCl_3$) δ = 1.2-1.4(m, 76H), 2.52 (q, -C**H₂**-SH, 8H), 3.75 (t, -O-C**H₂**-, 8H). **^{13}C NMR** (400 MHz, $CDCl_3$)**:** δ =24.8, 25.9, 28.6, 29.3, 29.6, 29.7, 29.7, 29.8, 32.5, 34.22, 63.7.**^{29}Si NMR** (400 MHz, $CDCl_3$)**:** δ = -81

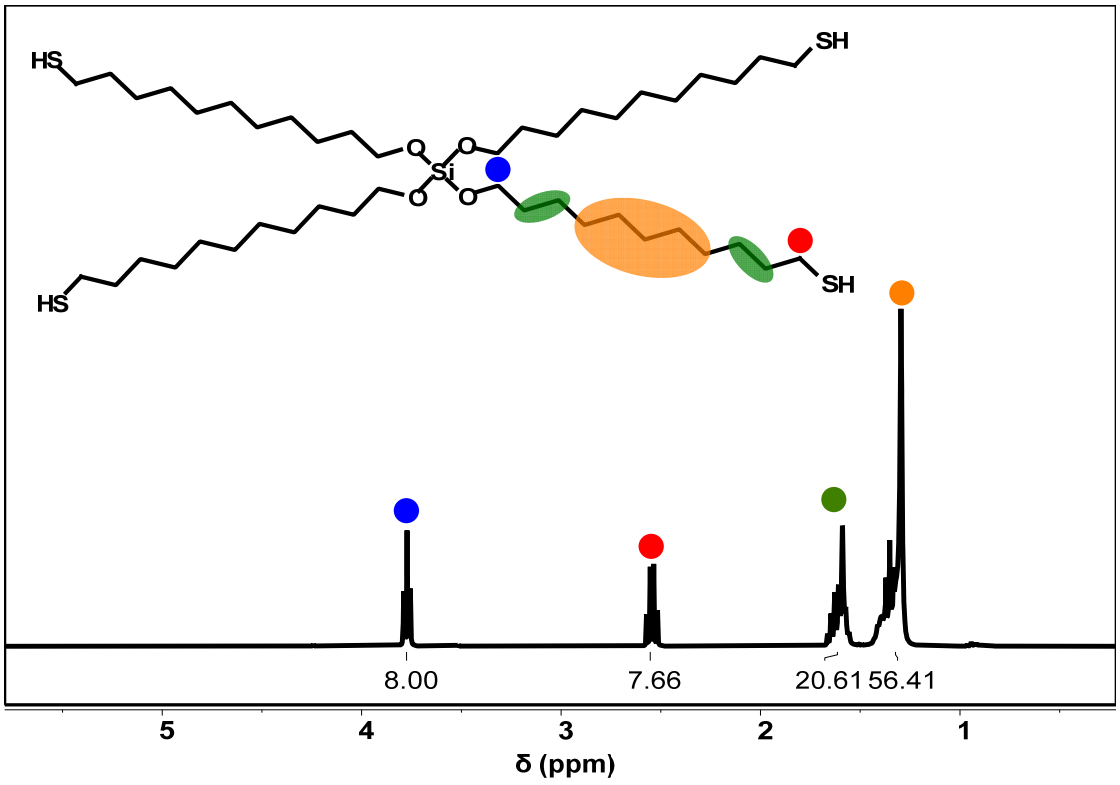
HS
SH
Si
O
HS
SH
8.00
7.66
20.61
56.41
5
4
3
2
1
δ (ppm)

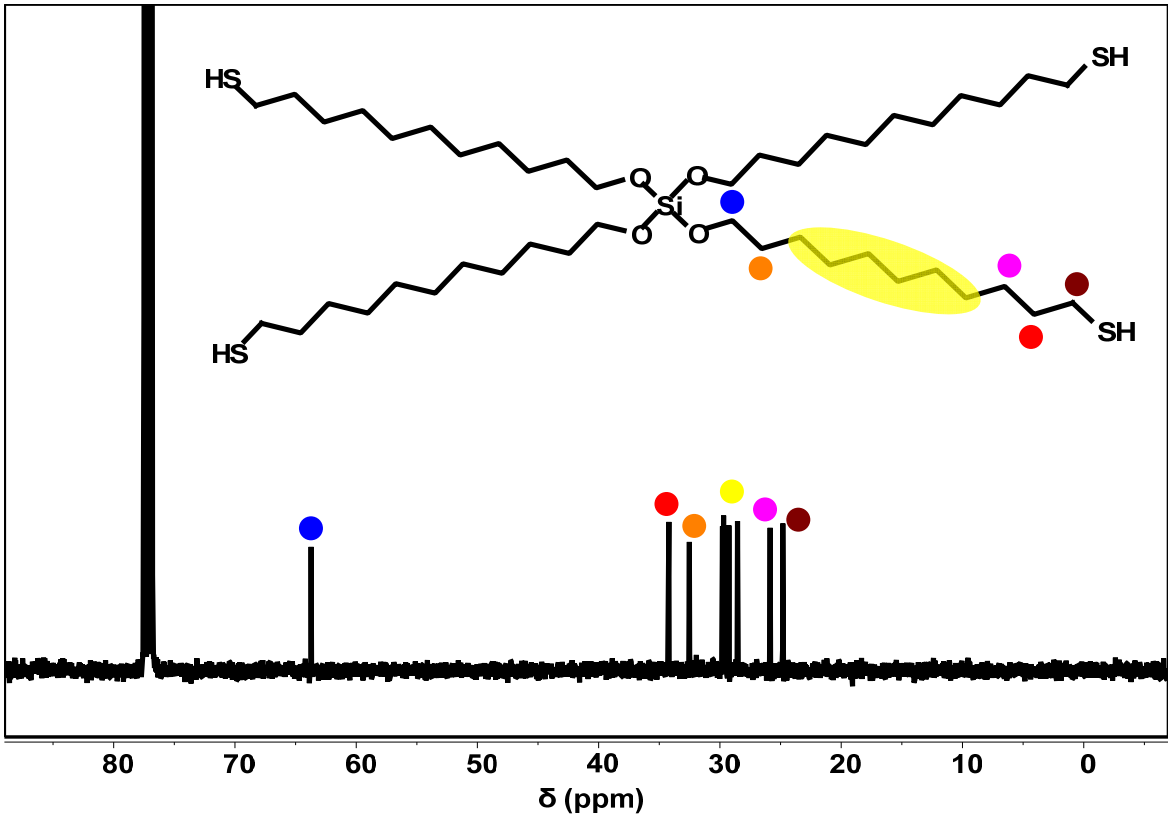
HS
SH
Si
O
HS
SH
80
70
60
50
40
30
20
10
0
δ (ppm)

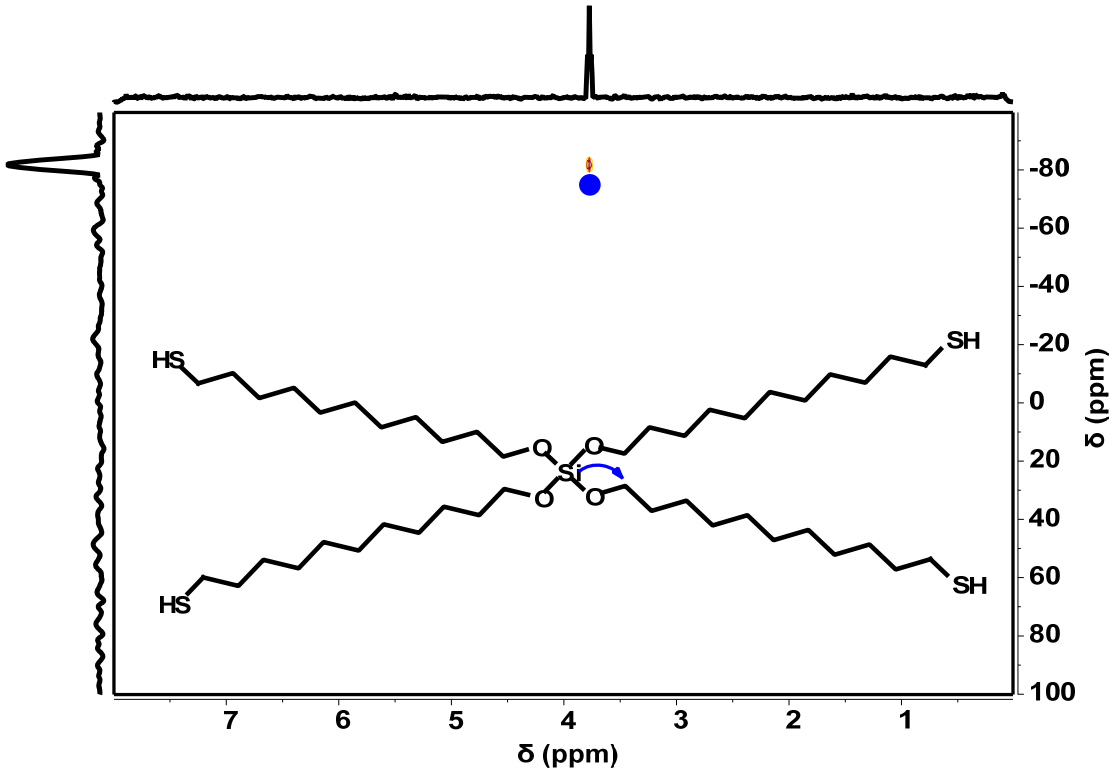

Figure S7. ^{1}H (Top), ^{13}C (Middle), and ^{1}H - ^{29}Si HMBC (Bottom) NMR spectra of tetrakis(11-mercaptoundecyl) silicate.

References

1. X. Meng, C. Crestini, H. Ben, N. Hao, Y. Pu, A. J. Ragauskas and D. S. Argyropoulos, *Nature Protocols*, 2019, **14**, 2627-2647.
2. J. V. Vermaas, L. D. Dellon, L. J. Broadbelt, G. T. Beckham and M. F. Crowley, *ACS Sustainable Chem. Eng.*, 2019, **7**, 3443-3453.
3. T. C. F. Gomes and M. S. Skaf, *J. Comput. Chem.*, 2012, **33**, 1338-1346.
4. A. D. MacKerell, D. Bashford, M. Bellott, R. L. Dunbrack, J. D. Evanseck, M. J. Field, S. Fischer, J. Gao, H. Guo, S. Ha, D. Joseph-McCarthy, L. Kuchnir, K. Kuczera, F. T. Lau, C. Mattos, S. Michnick, T. Ngo, D. T. Nguyen, B. Prodhom, W. E. Reiher, B. Roux, M. Schlenkrich, J. C. Smith, R. Stote, J. Straub, M. Watanabe, J. Wiórkiewicz-Kuczera, D. Yin and M. Karplus, *J Phys Chem B*, 1998, **102**, 3586-3616.
5. A. P. Thompson, H. M. Aktulga, R. Berger, D. S. Bolintineanu, W. M. Brown, P. S. Crozier, P. J. in 't Veld, A. Kohlmeyer, S. G. Moore, T. D. Nguyen, R. Shan, M. J. Stevens, J. Tranchida, C. Trott and S. J. Plimpton, *Comput. Phys. Commun.*, 2022, **271**, 108171.
6. S. Youssefian and N. Rahbar, *Sci. Rep.*, 2015, **5**, 11116.
7. E. E. Gorton Carruth, *Bond Energies*, Tennessee: Southwestern, 2002.